Chen et al. *Microsystems & Nanoengineering* (2026)12:42
https://doi.org/10.1038/s41378-025-01145-5

Microsystems & Nanoengineering
www.nature.com/micronano

ARTICLE Open Access

A magnetically actuated robotic capsule endoscope for in-situ visualization and microneedle-mediated targeted drug delivery in gastrointestinal tract

Weiyuan Chen[1,2], Jianbo Sui[1]✉, Xiaobiao Cao[1], Jiahao Huang[1], Fuqian Chen[3], Ke Zhao[3], Yuanyuan Li[3], Xiaxu Liu[3], Zhishan Yuan[1], Jinxiu Zhang[2], Lelun Jiang[3]✉, Xi Xie[3,4] and Chengyong Wang[1]

Abstract

Capsule endoscopy has revolutionized gastrointestinal (GI) diagnosis but is limited to imaging, often requiring invasive procedures for subsequent therapy. This work presents a magnetically actuated robotic capsule endoscope (MARCE) that integrates controllable magnetic navigation, real-time visualization, and targeted drug delivery via microneedle patches to bridge the gap between diagnosis and therapy. The MARCE features a retractable micro-camera for continuous monitoring of the GI tract, dual-layer hyaluronic acid microneedle patches enabling multi-point drug administration, and an electrothermally triggered protective cover to prevent premature dissolution in GI fluids. Sized similarly to conventional clinical capsules (11.8 mm in diameter and 21.5 mm in length), the MARCE demonstrates controlled epinephrine release from its microneedle patches (up to 0.4 mg) and provides sufficient magnetic actuation force (~0.58 N) and torque (~18.4 N mm) for intestine locomotion and penetration. Driven by a custom-developed electromagnetic actuation system, the MARCE achieves precise 3D locomotion with an average positional error <1.5 mm controlled microneedles penetration (with a peak force of 0.15 N), and successful drug delivery across multiple lesions in ex-vivo porcine intestinal tissue. This integrated platform streamlines diagnostic-therapeutic workflows, offering a minimally invasive solution for GI disorders such as bleeding, with potential to enhance patient comfort and treatment precision.

Introduction

Gastrointestinal diseases, including gastrointestinal inflammation, ulcers, bleeding, infections, and cancer, are prevalent clinical diseases with high morbidity and contribute to approximately 10% of deaths in the United States[1]. Gastroenteroscopy enables direct visualization of the gastrointestinal tract for accurate diagnosis. Traditional diagnostic approaches involve inserting an invasive endoscope through natural orifices (the mouth or anus), which can cause patient discomfort and pain. Moreover, examining the small intestine—on average 7 meters long and distant from natural orifices—remains technically challenging[2,3]. In 1995, Swain et al. introduced the concept of a capsule endoscope—a compact, swallowable device capable of passively traversing the gastrointestinal tract while capturing images[4]. In 2000, the capsule endoscope was first successfully used in clinical trials and has since gained widespread acceptance due to its ease of use and noninvasive nature[5–7]. However, current capsule endoscopes are limited to imaging only. Any needed treatment during examination requires additional procedures with traditional endoscopes, making the

Correspondence: Jianbo Sui (jianbo_sui@hotmail.com) or Lelun Jiang (jianglel@mail.sysu.edu.cn)
[1]State Key Laboratory for High Performance Tools, Guangdong Provincial Key Laboratory of Minimally Invasive Surgical Instruments and Manufacturing Technology, School of Electromechanical Engineering, Guangdong University of Technology, Guangzhou, China
[2]School of Aeronautics and Astronautics, Shenzhen Campus of Sun Yat-sen University, Shenzhen, China
Full list of author information is available at the end of the article

© The Author(s) 2026
Open Access This article is licensed under a Creative Commons Attribution-NonCommercial-NoDerivatives 4.0 International License, which permits any non-commercial use, sharing, distribution and reproduction in any medium or format, as long as you give appropriate credit to the original author(s) and the source, provide a link to the Creative Commons licence, and indicate if you modified the licensed material. You do not have permission under this licence to share adapted material derived from this article or parts of it. The images or other third party material in this article are included in the article's Creative Commons licence, unless indicated otherwise in a credit line to the material. If material is not included in the article's Creative Commons licence and your intended use is not permitted by statutory regulation or exceeds the permitted use, you will need to obtain permission directly from the copyright holder. To view a copy of this licence, visit http://creativecommons.org/licenses/by-nc-nd/4.0/.

diagnostic process more complex and increasing patient discomfort[8].

Research efforts have increasingly focused on integrating robotic technology into capsule endoscopes, transforming passive diagnostic devices into robotic capsule endoscopes (RCEs) with active therapeutic capabilities[9]. Various functionalities have been explored, such as emitting light of a specific wavelength for photodynamic therapy[10], releasing a surgical clip for intestinal hemostasis[11], inflating a silicone balloon to achieve hemostasis for the intestine by tamponade effect[12], self-expanding[13] or self-orienting[14,15] to penetrate soluble drug-loaded needles, and injecting drugs through high-pressure microjets[16] have been studied. However, these systems often lack active locomotion behaviors, limiting their ability to perform targeted drug delivery at specific lesions. When combined with magnetic actuation technology, RCEs can accomplish precise drug delivery. For example, by utilizing magnetic force to expand[17,18], squeeze[19], and vibrate[20] a drug-loaded chamber to trigger release, or by incorporating mechanical components such as ratchet[21], lead screw[22], and crank connecting rod[23] to leverage magnetic torque for actuation. Despite these advancements, the aforementioned RCEs offer only therapeutic functions and do not include video diagnostic capabilities.

For the treatment of intestinal bleeding, multi-point drug injection is commonly employed[24,25]. However, the use of traditional needles poses a safety risk of intestinal wall perforation during drug administration. Soluble drug-loaded microneedles offer a safer alternative for drug delivery, enabling large-area multi-point drug delivery through a single penetration procedure[26]. Among existing studies on RCE for delivering soluble drug-loaded microneedle patches, various mechanisms have been explored, including pH-responsive release[27,28], gastric juice dissolution[29], or electrothermal actuation[30] to deploy the patches within the gastrointestinal tract. Nevertheless, these approaches lack the precision necessary for targeted drug delivery to specific lesions. Furthermore, although magnetically actuated RCE systems have been proposed[31,32], none currently integrate video feedback, thereby failing to fulfill the clinical demand for combined diagnostic and therapeutic functionalities.

Herein, we present a novel magnetically actuated robotic capsule endoscope (MARCE) designed for in-situ visualization and microneedle-mediated targeted drug delivery within the gastrointestinal tract. MARCE is equipped with a retractable micro-camera at its front end for real-time imaging of the gastrointestinal tract, along with two drug-loaded microneedle patches intended for targeted drug delivery for gastrointestinal bleeding, addressing the therapeutic limitation of traditional capsule endoscopes. The microneedle patches are shielded by a controlled-release protective cover that prevents exposure to gastrointestinal fluids. Under the magnetic actuation provided by a self-developed external electromagnetic actuation (EMA) system, MARCE can be precisely navigated to the target lesion. Upon arrival, the protective cover is electrically triggered to detach, allowing the microneedle patches to penetrate the lesion and deliver drugs via magnetic actuation. This platform streamlines workflows, reduces patient discomfort, and demonstrates potential for advancing the treatment of gastrointestinal diseases.

Results and discussion

Conceptual design of MARCE

MARCE is designed to integrate magnetic navigation, visualized diagnosis, and targeted drug delivery within the gastrointestinal tract, as illustrated in Fig. 1a. It primarily consists of magnetized NdFeB magnets for controllable locomotion, a retractable micro-camera enabling real-time monitoring, dual-layer drug-loaded microneedle patches protected by a soluble cover for multi-site targeted delivery, and tethered wires for power supply, signal transmission, and easy retrieval. Driven by an external electromagnetic actuation (EMA) system, the MARCE achieves precise 3D locomotion and orientation control (e.g., yaw, pitch, and axial movement) via magnetic force and torque, enabling accurate navigation to target lesions (Fig. 1b). Upon arrival, the protective cover is released by an electrothermal trigger, and magnetic actuation drives the microneedle patches to penetrate the lesion, where the hyaluronic acid microneedles gradually dissolve to release drugs (e.g., epinephrine for hemostasis), enabling localized therapy (Fig. 1c). This design of MARCE offers advantages of non-invasiveness, minimal patient discomfort, precise mm-level targeting (average positional error <1.5 mm), multi-point drug delivery, and a streamlined single-procedure diagnostic-therapeutic approach, overcoming the limitations of traditional capsule endoscopes that lack therapeutic capabilities.

Assembly and characterization of MARCE

Figure 2a shows the MARCE, which has a diameter of 11.8 mm and a length of 21.5 mm—similar to existing commercial capsule endoscopes (Table S1). Figures 2b–d and S1 present its cross-sectional schematic, assembled components, exploded view, and design drawing. Magnets A and B form a magnetic spring that supports the 2-mm micro-camera at the front end, where two microneedle patches are integrated. The protective cover is pre-compressed using two helical springs and held in place by 0.15-mm nichrome wires. All components are enclosed in outer shells bonded with medical-grade adhesive. The shells are 3D-printed from biocompatible photosensitive polymer E-shell 200[33,34].

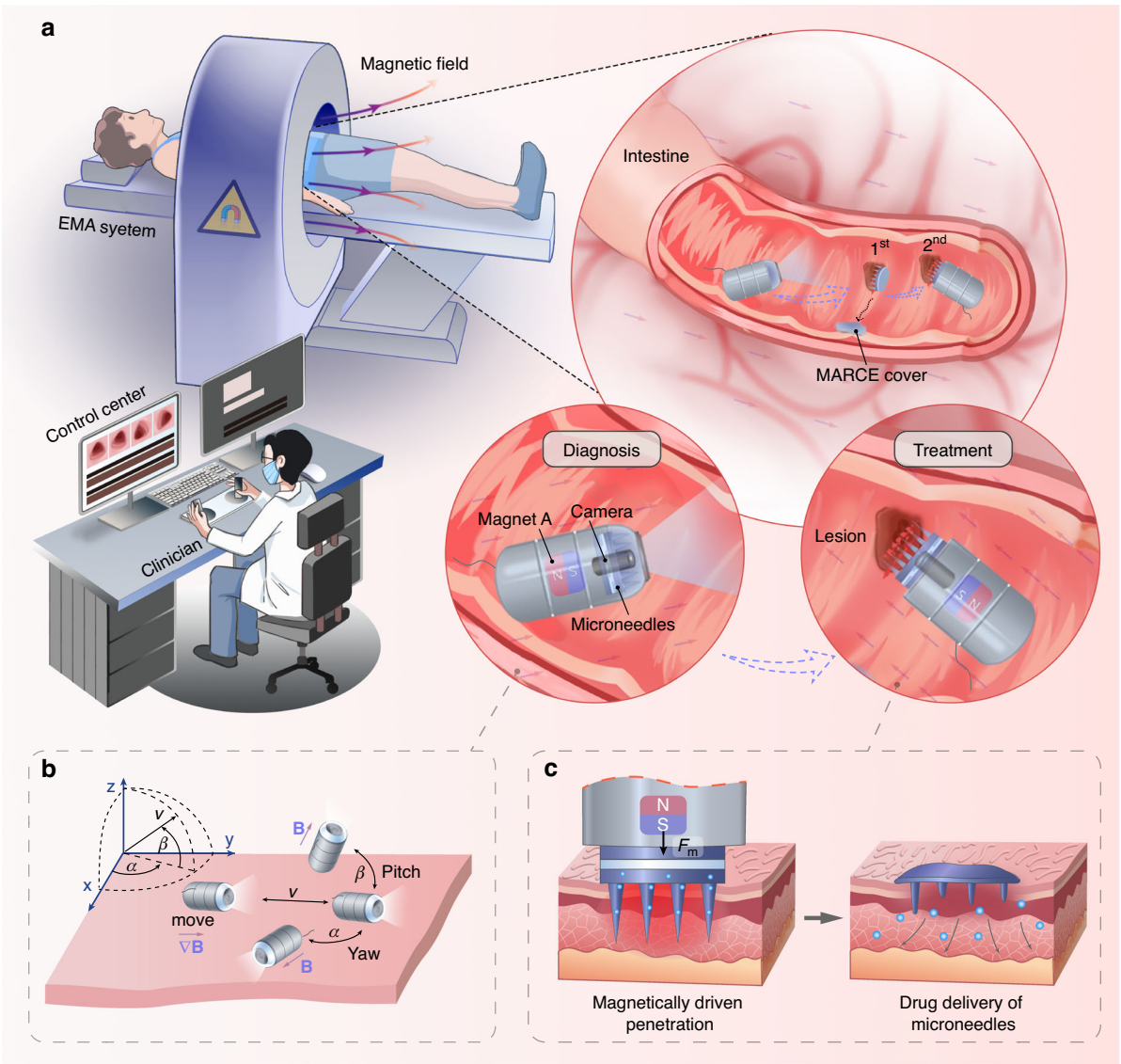


Fig. 1 Conceptual design of MARCE and EMA system. a Schematic illustration of MARCE for magnetic navigation, visualized diagnosis, and targeted drug delivery under the actuation by the EMA system. **b** Schematic illustration of 3D magnetic locomotion and orientation control (e.g., yaw, pitch, and axial movement) of the MARCE. **c** Schematic illustration of drug delivery mechanism via the dissolvable microneedle patch

To target multiple adjacent lesions[35–37], two hyaluronic acid-based dissolvable microneedle patches are stacked at the front, separated by a perforated PDMS pad to protect the second patch (Fig. 2e). Each patch is approximately 9 mm in diameter and contains 30 conical microneedles (Fig. 2f), each about 700 μm in height (Fig. 2g). During delivery, the first patch and PDMS pad are removed together from the second patch, followed by separating the second microneedle patch from the holder, as shown in Fig. 2h.

A micro camera with a retractable mechanism is integrated into the MARCE for in-situ observation without interfering with microneedle patches during gastrointestinal mucosal puncture. The micro-camera (2 mm in diameter and 5 mm in length), equipped with 4 LEDs and a resolution of 400 × 400 pixels (Fig. S2), enables real-time monitoring. The extension and retraction of the camera due to the magnetic spring are shown in Video S1. The camera, positioned dynamically by a magnetic spring, avoids obstructing its own vision field and the penetration of microneedle patches during deployment. The magnetic spring uses the repulsion between two NdFeB magnets (magnet A assembled within the capsule and magnet B attached to the camera) to achieve a low elastic coefficient of 7.29 mN/mm within a displacement range d_s of 2.3–3.7 mm (Fig. 2i). Simulations and measurements confirm the effectiveness of the magnetic force F_m in

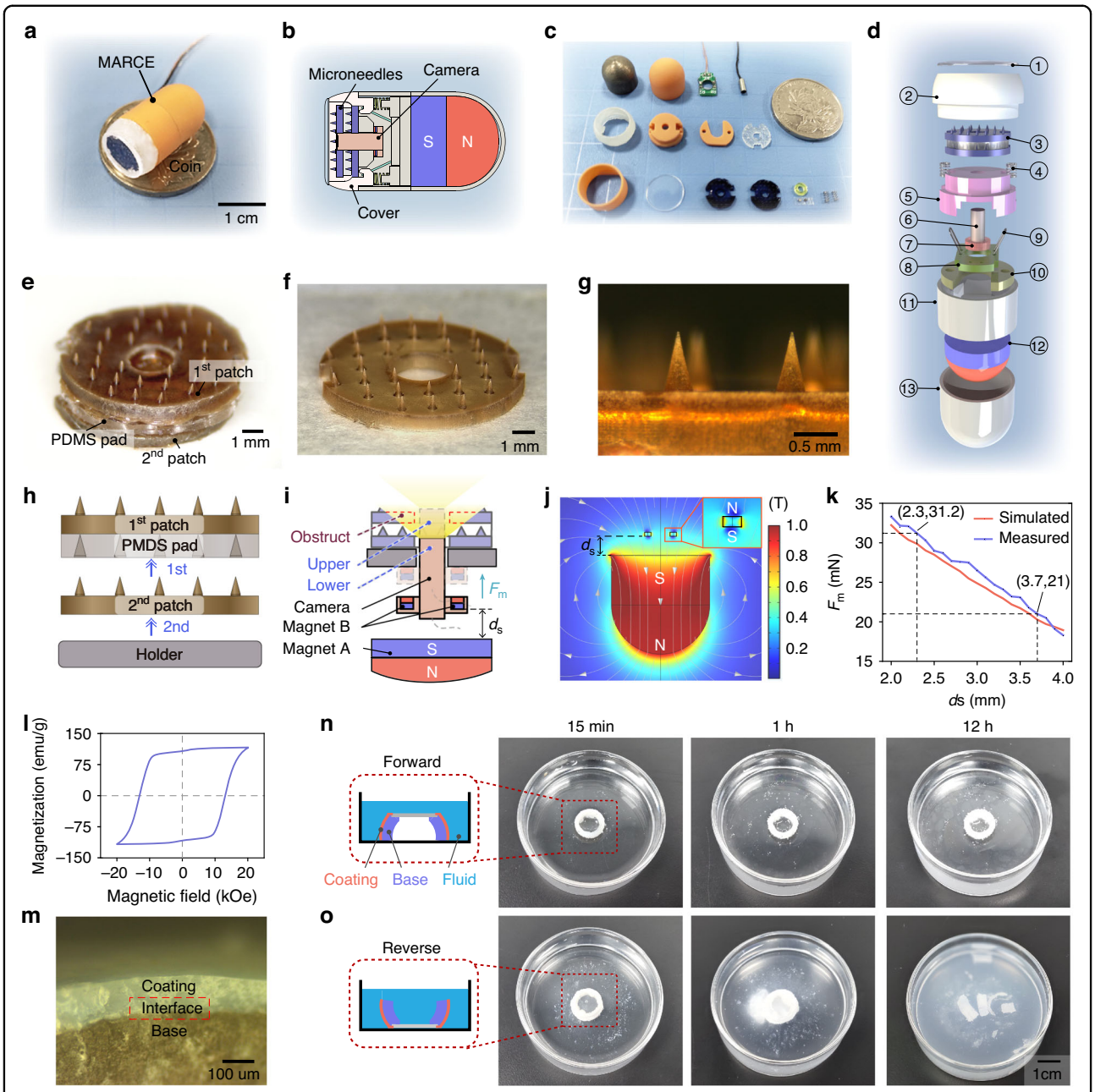


Fig. 2 Assembly and characterization of MARCE. a Image of MARCE. **b** Cross-sectional schematic of MARCE. **c** Components of MARCE. **d** Exploded view of MARCE. 1. Transparent lens, 2. Cover base, 3. Microneedle patches, 4. Spring, 5. Microneedle patch holder, 6. Camera, 7. Micromagnet holder, 8. Circuit board, 9. Nichrome wire, 10. Backing plate, 11. Middle shell, 12. Magnet A, 13. End shell. **e** Two microneedle patches. **f** A microneedle patch. **g** The magnified view of microneedles. **h** Sequential separation diagram of two microneedle patches. **i** Illustration of the retractable camera. **j** Finite element analysis of the magnetic flux density of the magnetic spring. **k** Simulated and measured results illustrating the relationship between the magnetic spring distance and magnetic force. **l** Magnetic hysteresis loop of NdFeB magnet. **m** Cross-sectional morphology of the PTFE-coated cover base. Dissolution behavior of the protective cover, without **n** and with **o** its inner surface exposure, in simulated intestinal fluid

driving the retractable mechanism (Figs. 2j, k and S3A). The hard magnetic hysteresis property of the NdFeB magnets (Fig. 2l) ensures the stability of magnetic spring. Notably, Magnet B is significantly smaller than Magnet A (1/2516 of its volume), minimizing internal magnetic interference. This design is ingenious, compact, and efficient, utilizing existing magnetic components within the MARCE.

Microneedle patches require a protective cover to prevent damage or contamination from gastrointestinal fluids

during MARCE transit to the lesion site. The protective cover comprises a transparent acrylic lens bonded to a base. The cover base is fabricated from a soluble material with an insoluble outer coating, ensuring it dissolves only after release when the inner surface contacts gastrointestinal fluid. Specifically, the cover base consists of 75% polyethylene oxide (PEO) and 25% Soluplus mixture, which are biocompatible and soluble[28]. The outer surface is coated with polytetrafluoroethylene (PTFE), selected for its low friction, chemical stability, and biocompatibility[38,39]. The cross-sectional morphology of the PTFE-coated cover base was observed using a scanning electron microscope, as shown in Fig. 2m, revealing a uniform and tightly adhered coating. Figure 2n, o shows the dissolution behavior of the protective cover, with and without its inner surface exposure to simulated intestinal fluid. The forward-placed cover remained intact after 12 h in simulated intestinal fluid, while the reverse-placed cover was almost completely dissolved. This indicates that the protective cover can resist dissolution before release and dissolve quickly after release.

Magnetically actuated locomotion performance of MARCE

An EMA system was custom-developed for the magnetic actuation of MARCE, as shown in Fig. 3a. This system comprises three mutually orthogonal pairs of Maxwell and Helmholtz coils aligned along the *X*, *Y*, and *Z* axes (Fig. 3b). The Maxwell coils generate gradient magnetic fields to propel MARCE movement via magnetic force, whereas the Helmholtz coils produce uniform fields to induce torque for yaw and pitch control. Through vector synthesis of these fields, the MARCE can be directly actuated to move freely within a three-dimensional space. The operator inputs desired locomotion behaviors via a joystick. The system computes the necessary current based on the input signal and delivers it to the respective coils, generating the required magnetic field to actuate the MARCE (Fig. 3c). To simplify the finite element analysis of the magnetic actuation of MARCE using the EMA system, the magnetic field distributions generated by a pair of Maxwell coils and a pair of Helmholtz coils were simulated (Figs. 3d–f and S3B, C). The distance between the Maxwell coil pair d is approximately $\sqrt{3}$ times the coil radius r, with input current flowing in opposite directions. Both simulated and measured magnetic forces acting on the MARCE along the x-axis almost linearly increase with the input currents, showing a similar trend (Figs. 3e and S4A). The distance between the Helmholtz coil pair d is equal to their radius r, and the input currents flow in the same direction. The simulated and experimental magnetic torques acting on the MARCE around the z-axis also exhibit a consistent increasing trend with respect to the input currents (Figs. 3g and S4B). The magnetic force and magnetic torque acting on the MARCE are proportional to the input current. When the maximum current of 10 A is applied, the measured magnetic force and torque reach 0.58 N and 18.4 N mm, respectively.

The locomotion of the MARCE, actuated by the EMA system, was evaluated within a tubular model covered with porcine intestinal tissue, as shown in Fig. 3h and Video S2. The MARCE can achieve forward movement driven by the magnetic force F_m, and can perform yawing and pitching behaviors through the magnetic torque T_m. To assess its maneuverability, tracks shaped like "*R*", "*C*", and "*E*" were 3D printed, and the MARCE was guided through these tracks by the magnetic field generated by the EMA system, as shown in Fig. 3i and Video S3. It can be observed that the MARCE successfully navigated through the intestine phantom. Figure 3j shows the trajectory error between the reference and actual trajectories of the MARCE locomotion along the "*R*" "*C*" "*E*" tracks. The average locomotion error across the entire trajectory was approximately 0.45 mm. Therefore, it is concluded that the MARCE proposed in this work can effectively and controllably navigate within the gastrointestinal tract under magnetic field control.

Drug delivery performance of MARCE

The protective cover of MARCE, preloaded with two compressed springs, is controllably released via an electrically triggered mechanism (Fig. 4a and Video S4). The MARCE employs nichrome wires soldered to a circuit board to mechanically secure cover-mounted humps (Fig. 4b). Upon application of voltage, resistive heating rapidly softens the humps until spring forces overcome their structural integrity, thereby ejecting the protective cover. Thermal activation experiments ($n = 5$, 37 ± 3 °C) demonstrated a voltage-dependent threshold, with reliable triggering occurring between 0.8 and 5 V (Fig. 4c). At voltages below 0.8 V, insufficient heating prevented cover release, while higher voltages accelerated activation. The optimal performance was achieved at 2.2 V, where the response delay was merely 1.07 s, requiring a minimum energy consumption of 3.1 J, which was therefore established as the operational voltage. Following cover ejection, MARCE precisely deploys drug-loaded microneedle patches to gastrointestinal lesions for targeted delivery. The thermal safety of MARCE was evaluated to ensure minimal risk upon opening of the protective cover, as shown in Fig. 4d–f. After cover ejection, the nichrome wires soldered to the circuit board remained encapsulated within MARCE, avoiding direct contact with the intestines and ensuring thermal safety. Temperature variations of the nichrome wire were recorded using a 0.25-mm thermocouple and showed rapid cooling to about 40 °C within 10 s in air after heating (Fig. 4d). The temperature of the ejected

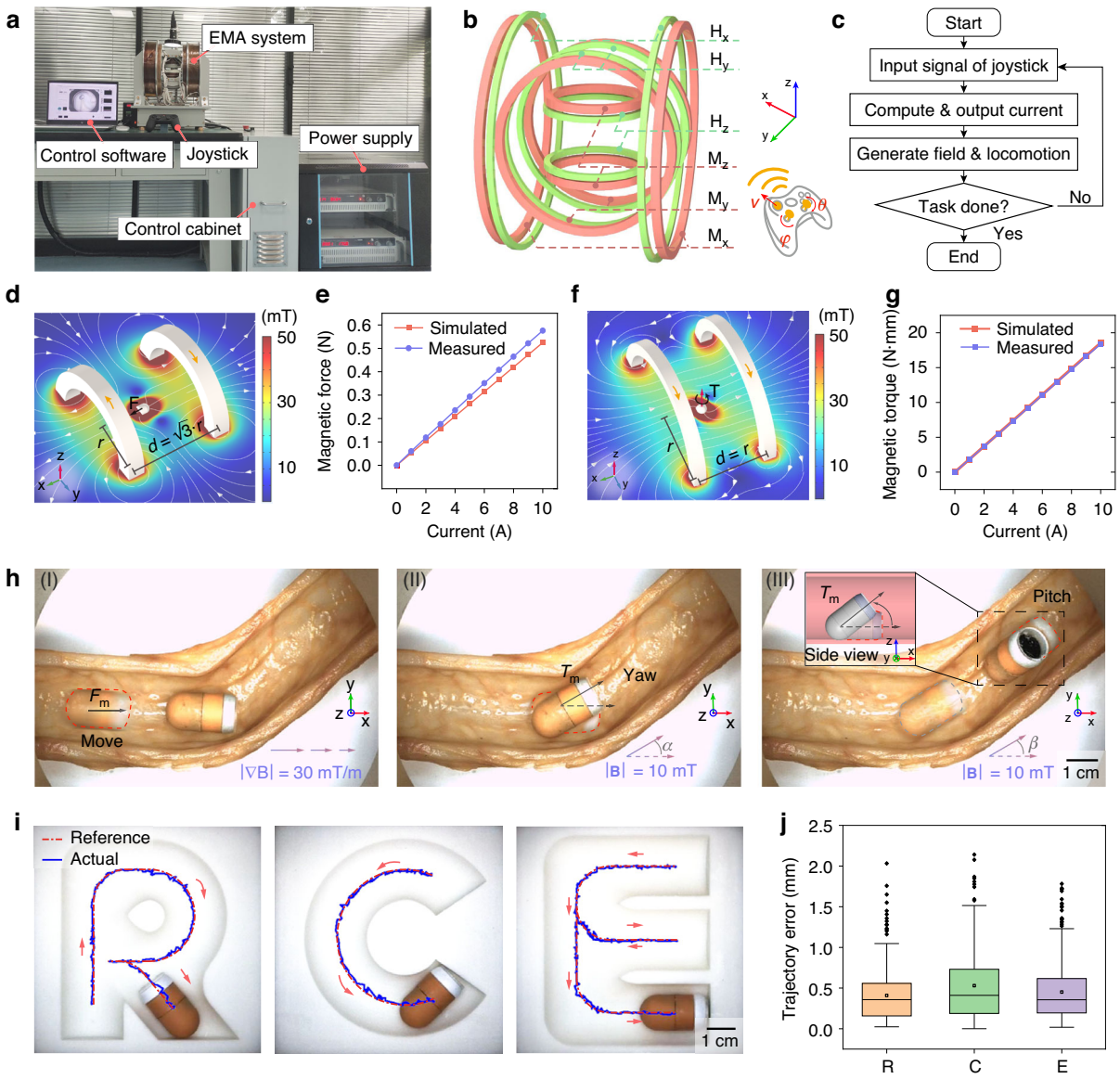


Fig. 3 Magnetically actuated locomotion of MARCE. a Image of EMA system. **b** Schematic of the electromagnetic coils configuration of the EMA system. $\mathbf{H}_x$, $\mathbf{H}_y$, and $\mathbf{H}_z$ represent the Helmholtz coils along *x*, *y*, and *z* axes, respectively; $\mathbf{M}_x$, $\mathbf{M}_y$, and $\mathbf{M}_z$ represent the Maxwell coils along *x*, *y*, and *z* axes, respectively. **c** Control procedure for magnetic actuation of MARCE using EMA system. **d** Finite element analysis of the magnetic flux density generated by a pair of Maxwell coils. **e** Simulated and measured magnetic forces under varying input currents. **f** Finite element analysis of the magnetic flux density generated by a pair of Helmholtz coils. **g** Simulated and measured magnetic torques under varying input currents. **h** Locomotion behaviors of the MARCE in the intestinal phantom under magnetic actuation using the EMA system. **i** Locomotion trajectories of the MARCE along "*R*" "*C*" "*E*" tracks. **j** Locomotion trajectory errors along the "*R*" "*C*" "*E*" tracks

protective cover was further measured via an embedded thermocouple (Fig. 4e), showing a peak of 37.7 °C (ambient: 36.7 °C) before stabilizing at 37.1 °C upon contact with tissue (Fig. 4f). Across 10 trials, temperature variations remain within 1.5 °C—well below biological safety thresholds[40]. This confirms no risk of thermal injury to gastrointestinal tissues.

The drug delivery performance of the microneedle patch loaded with epinephrine into the small intestinal tissue of swine was investigated, as shown in Fig. 4g–j. Epinephrine is a drug commonly used for treating gastrointestinal bleeding[24,37]. The microneedle patch was advanced and successfully penetrated the intestinal tissue, remained in place for epinephrine release as the hyaluronic acid matrix dissolved, and was subsequently retracted, as shown in Fig. 4i. The amount of released drug increased gradually with the dissolution time of the microneedle patch, eventually reaching the total drug load

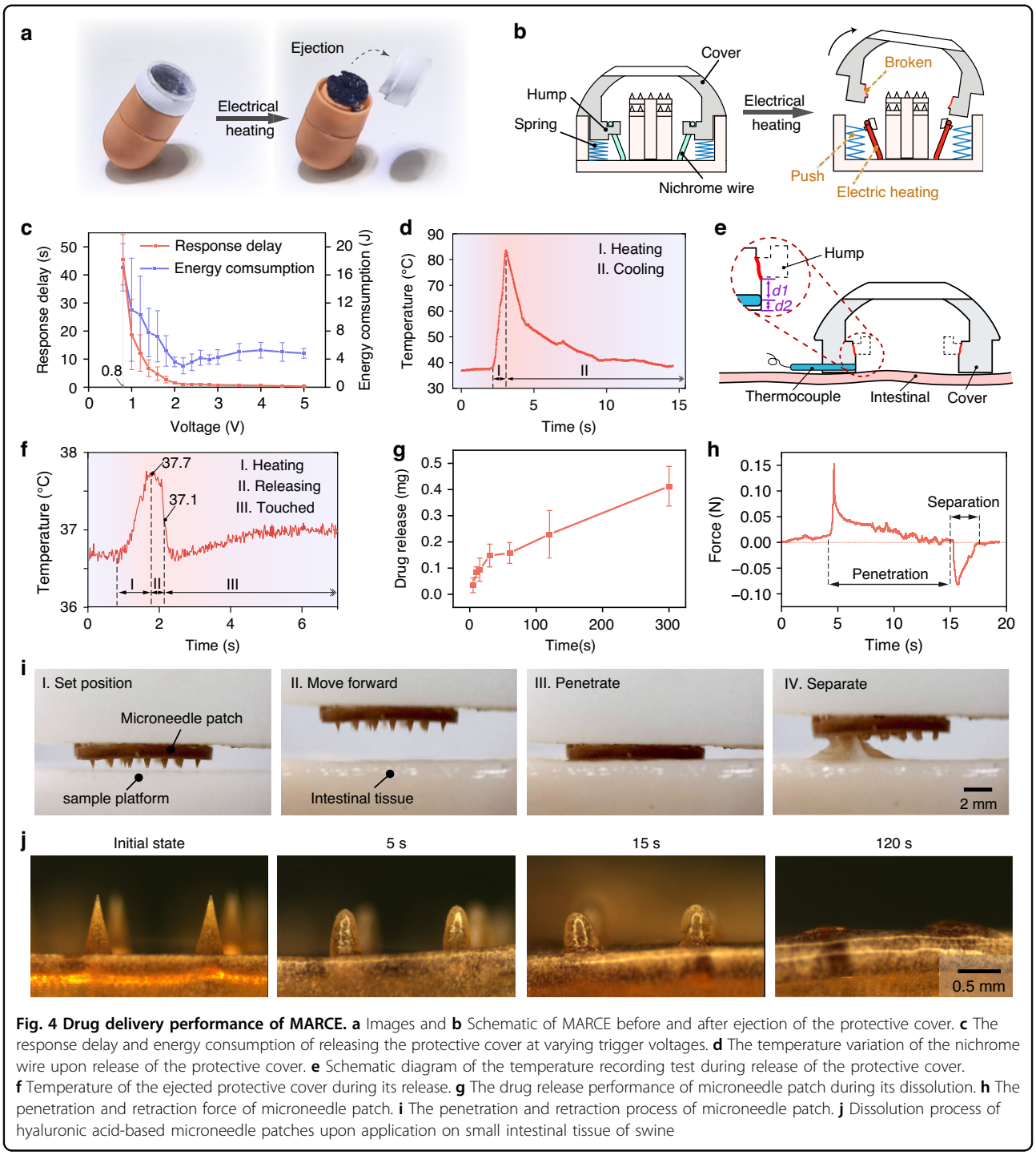


Fig. 4 Drug delivery performance of MARCE. a Images and **b** Schematic of MARCE before and after ejection of the protective cover. **c** The response delay and energy consumption of releasing the protective cover at varying trigger voltages. **d** The temperature variation of the nichrome wire upon release of the protective cover. **e** Schematic diagram of the temperature recording test during release of the protective cover. **f** Temperature of the ejected protective cover during its release. **g** The drug release performance of microneedle patch during its dissolution. **h** The penetration and retraction force of microneedle patch. **i** The penetration and retraction process of microneedle patch. **j** Dissolution process of hyaluronic acid-based microneedle patches upon application on small intestinal tissue of swine

of approximately 0.4 mg within 5 min, as shown in Fig. 4g. Clinical studies typically administer 0.05 to 0.15 mg of epinephrine for gastrointestinal bleeding[24,38]. The microneedle patch can deliver up to 0.4 mg, meeting the standard clinical dose and allowing flexibility for dosage adjustments. Clinicians can, based on the patient's actual medication needs, instruct the patient to adjust their lying direction. This allows the intestinal fluid to cover the microneedle patch, causing it to dissolve and deactivate in the intestinal fluid, thereby terminating the drug delivery process. Additionally, the dissolution process of the microneedle patch was monitored and showed complete dissolution within 2 min, demonstrating a rapid drug delivery capability (Figs. 4j and S5). The penetration force

of microneedle patch was also investigated using a self-developed mechanical testing system (Figs. 4h and S6). As the microneedle patch penetrated the intestinal tissue, the push force quickly increased to a peak of 0.15 N and then dropped rapidly to nearly zero within 10 s, indirectly indicating tissue penetration and microneedle dissolution. Subsequently, a maximum adhesion force of 0.08 N was observed during the retraction of the microneedle patch.

In-situ visualization and targeted drug delivery of MARCE under magnetic actuation

The entire process of magnetic navigation, in-situ visual observation, and targeted drug delivery of the MARCE was systematically investigated in an intestine phantom, as shown in Fig. 5a and Video S5. Under magnetic actuation of EMA system, the MARCE navigated toward the marked target (Fig. 5a-i). Upon approaching the target lesion, the orientation of the MARCE was adjusted using magnetic torque, and subsequently, the protective cover was ejected via an electrical trigger (Fig. 5aII-III). Subsequently, the MARCE was fine-tuned to position the microneedle patch accurately on the target lesion. The first microneedle patch was advanced toward the lesion with consistent pressure for a predetermined duration using magnetic force of the MARCE (Fig. 5a-IV). After successful delivery, the MARCE reversed direction to detach the patch from the capsule body. If another nearby lesion was detected, the second patch was administered using the same procedure (Fig. 5a-V). Finally, after completing the delivery, the MARCE was guided away from the lesion area (Fig. 5a-VI). These results show that the MARCE can effectively deliver microneedle patches to specific sites within the intestinal phantom through magnetic actuation.

The magnetic navigation behaviors, in-situ visualization, and microneedles-based targeted drug delivery capabilities of the MARCE were also evaluated in a segment of porcine small intestine, as shown in Fig. 5b and Video S6. The operator magnetically controlled the locomotion of the MARCE based on real-time images captured by the integrated micro-camera via a joystick. The MARCE successfully delivered two microneedle patches to target lesions in an ex vivo small intestine. The average position errors between the patch centers and the lesion centers for the first and second targets were 1.36 mm and 1.43 mm (Fig. 5c), respectively. Since most intestinal bleeding lesions are smaller than 5 mm[35,36] and the microneedle patches have a diameter of 9 mm, they can effectively cover the target lesions. Histological analysis confirmed that the microneedle patch successfully penetrated the mucosal layer under magnetic actuation, validating the feasibility of drug delivery (Fig. 5d). Additionally, the locomotion resistance of the MARCE under various intestinal conditions was measured (Fig. S7), with a maximum force of 0.309 N under a locomotion speed of 20 mm/s selected as reference (Fig. 5e). Since MARCE can generate a magnetic driving force of 0.58 N, it is expected to operate effectively across different intestinal environments. A potential clinical challenge is gastrointestinal fluid accumulation due to gravity, which may reduce delivery effectiveness of microneedle patches by covering the lesion. Adjusting the position of patient (e.g., supine or lateral) can help access the target area and maintain patch functionality.

Conclusions

We present a novel MARCE that integrates magnetic navigation, real-time visualization, and microneedle-mediated targeted drug delivery within the gastrointestinal tract, addressing the limitation of conventional capsule endoscopes that lack therapeutic functionality. The MARCE, driven by a self-developed electromagnetic actuation (EMA) system, enables magnetically guided locomotion within the gastrointestinal tract, allowing for targeted delivery of drug-loaded microneedle patches to specific lesions. Its design incorporates a retractable micro-camera for continuous visual feedback and a protective cover that shields the microneedles from gastrointestinal fluids, thereby ensuring both diagnostic accuracy and therapeutic efficacy. The MARCE (11.8 mm diameter, 21.5 mm length) is dimensionally compatible with clinically used capsule endoscopes. Ex vivo studies demonstrate its capability to deliver microneedle patches to target lesions with an average positional error of less than 1.5 mm, while releasing drugs (e.g., epinephrine) in a controlled manner. The EMA system provides precise locomotion control, with measured magnetic force (0.58 N) and torque (18.4 N mm) sufficient to meet both locomotion and intestine penetration requirements. This work marks a key step toward minimally invasive platforms combining diagnosis and therapy for gastrointestinal diseases, offering improved patient comfort and treatment precision. Future clinical translation may revolutionize management of gastrointestinal disorders such as bleeding and inflammation.

Experimental

Materials preparation

Hyaluronic acid (Mw 240 kDa) was purchased from Focusfreda Biotech Co., Ltd. (China). Epinephrine (Mw 183.2 Da) was supplied by Titan Scientific Co., Ltd. (China), and methylene blue was supplied by Biohonor Co., Ltd. (China). The PDMS was prepared using Sylgard 184 (Dow Corning, USA). Ultrapure type I water was delivered by the PURELAB Classic system (ELGA LabWater, UK). Potassium phosphate monobasic, NaOH (sodium hydroxide), PEO (polyethylene oxide, Mv 300 kDa), PTFE dispersion (polytetrafluoroethylene, 60%

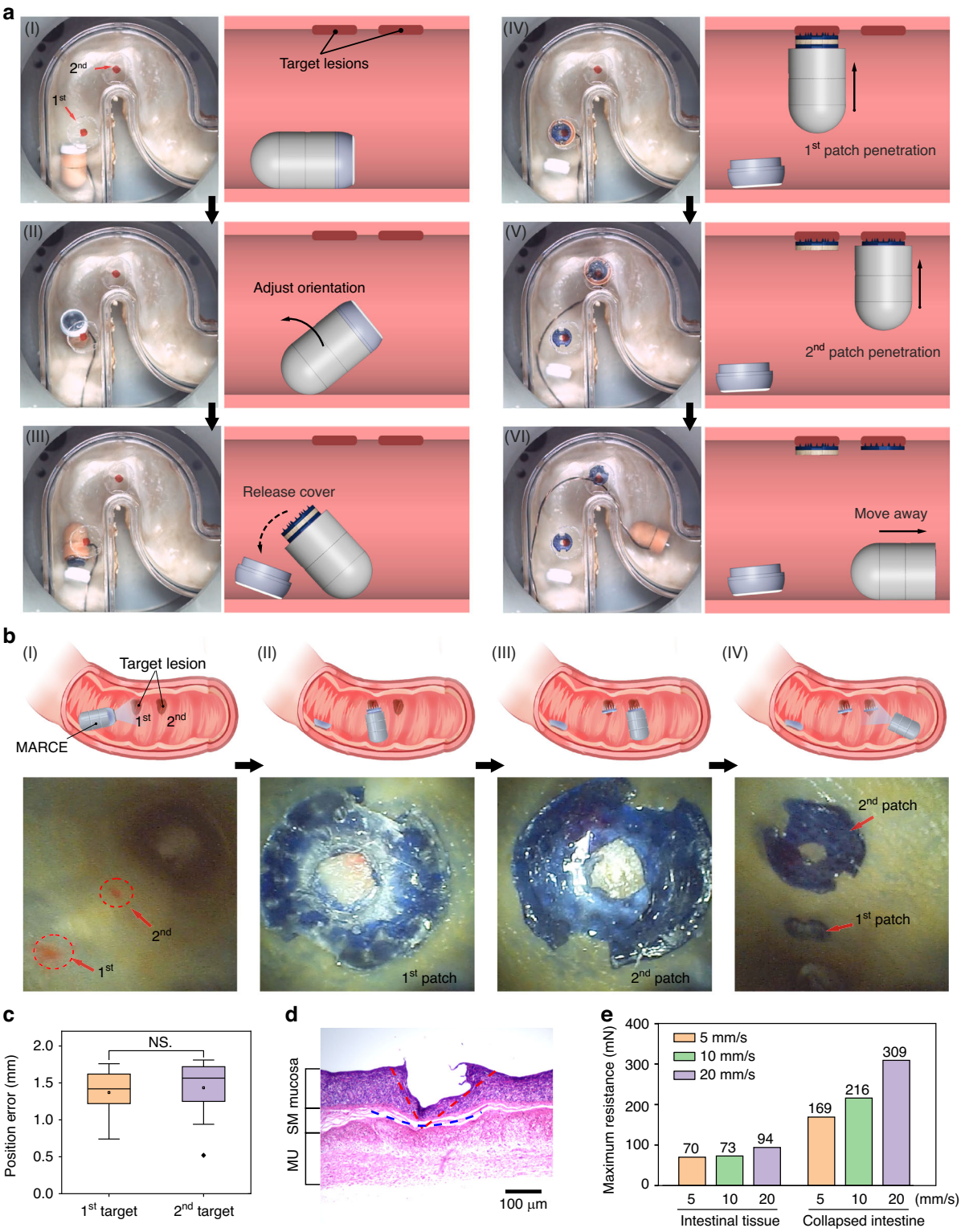


Fig. 5 Magnetic navigation, in-situ visualization, and microneedles-based targeted drug delivery of MARCE. a The process of magnetic navigation, in-situ observation, and targeted drug delivery of the MARCE in an intestine phantom. **b** The magnetic navigation, in-situ visualization, and microneedles-based targeted drug delivery of the MARCE in a segment of porcine small intestine. **c** The average position errors between the patch centers and the lesion centers. $N = 10$, NS. means not significant. **d** Histological analysis of the small intestine following penetration of microneedle patch. SM submucosa, Mu muscularis externa. **e** Maximum locomotion resistance of the MARCE under various intestinal conditions

wt), and aluminum dihydrogen phosphate were obtained from Macklin Biochemical Co., Ltd. (China). Soluplus (polyvinyl caprolactam-polyvinyl acetate-polyethylene glycol graft copolymer) was provided by BASF. Master molds were provided by Boston Micro Fabrication Co., Ltd. (China). Magnet A (N52 permanent magnet, 10.6 mm in both diameter and length, axially magnetized and featuring a hemispherical head at one end) and magnet B (N52 permanent magnet, 0.7 mm in diameter and 0.4 mm in length, axially magnetized) were fabricated by Jiaozuo Jicheng Magnetoelectric Co., Ltd., China. The shell of the MARCE was made of the photosensitive polymer E-shell 200 (EnvisionTEC, Germany) through 3D printing. Porcine intestines were obtained from a local slaughterhouse.

Fabrication of MARCE

Fabrication of microneedle patch

A hyaluronic acid-based dissolving microneedle patch and a PDMS pad were fabricated using micro-molding method. Fig. S8A illustrates the process: PDMS solution was poured into a polyacrylic resin mold, cured at 80 °C for 2 h, and used as a soft female mold. A 6% hyaluronic acid solution containing the drug was poured into this mold, vacuum-treated, and periodically replenished during drying to prevent shrinkage. The final microneedle patch was successfully fabricated in 30 h at room temperature. The PDMS pad (Fig. S8B) was fabricated in a similar process and subsequently plasma-treated to increase adhesion. Double-sided tape with precisely controlled adhesion force was used to attach the microneedle patches to the PDMS pad and holder (Fig. S9).

Fabrication of protective cover

The protective cover consisted of a transparent acrylic lens bonded to a base. The base was made by mixing 75% PEO and 25% Soluplus using a screw extruder (Process 11, ThermoFisher Scientific, Germany) at 145 °C and 30 rpm. The fabrication process of the cover base is shown in Fig. S10. A PDMS mold was firstly created by pouring PDMS solution into a 3D-printed master mold, curing it at 80 °C for 1 h (Fig. S10A). The mold was then inverted and the base material was loaded through the feed opening and pressed via injection molding (Fig. S10B). After heating at 140 °C for 15 min and followed by cooling, the soluble base was obtained. Its outer surface was coated with an insoluble PTFE dispersion containing aluminum dihydrogen phosphate.

Assembly of MARCE

The assembling components and exploded view of MARCE prototype are shown in Fig. 2c and Fig. 2d. Magnet A was employed to provide magnetic actuation. Together, Magnet A and Magnet B formed a magnetic spring system designed to support the micro camera. At the front end of the MARCE, a micro camera (OV6946, Anyview Co., Ltd., China) with a diameter of 2 mm was integrated along with two microneedle patches. The protective cover was pre-compressed using two helical springs (1.45 mm in diameter and 3.18 mm in length, Lee Spring Co., Ltd., USA) and secured in place by nichrome wires with a diameter of 0.15 mm. The outer shells of all components were bonded together using a medical-grade adhesive (Loctite 435, Henkel Investment Co., Ltd., China)[18].

Dissolution and thermal safety tests of protective cover

Dissolution test

The solubility of the protective cover was evaluated in a simulated intestinal environment, which was prepared by dissolving 0.68 g of monobasic potassium phosphate and 0.09 g of NaOH in 100 mL of water. The protective cover was placed in a petri dish in the forward and reverse orientations. 25 mL of simulated intestinal fluid at 37 °C was added to the petri dish, and the samples were incubated in a temperature-controlled oven at 37 °C. Observations were conducted at 15 min, 1 h, and 12 h, respectively.

Thermal safety test

Two thermocouples (diameter: 0.25 mm) were inserted into the MARCE, one in direct contact with the nichrome wire and the other positioned near the incision of the protective cover (Fig. 4e). The temperature variations were recorded using a data acquisition module (OMDAQ-USB-2401, Omega Engineering Inc., USA) during the energization of the nichrome wire, which triggered the release of the protective cover.

Mechanical testing

Retractable force of camera

A mechanical testing system was developed, as shown in Fig. S6. It comprises a positioning stage that drives the pusher vertically and a dynamometer to measure the loading force. The MARCE, after removal of its protective cover and microneedle patches, was assembled on the sample platform. Subsequently, the retractable force of the camera due to the magnetic spring generated by Magnet A and Magnet B was measured using the mechanical testing system.

Penetration force of microneedle patch

The penetration test was conducted using the mechanical testing system, as illustrated in Figs. S6 and 4i. The microneedle patch was moved toward the intestinal tissue fixed on the sample platform, held in place for 10 s, and then retracted. The loading and unloading speeds

were set at 5 mm/s. The penetration force and loading displacement were simultaneously recorded.

Magnetic force and torque on the MARCE

The magnetic force acting on the MARCE was tested using a tensile dynamometer in the EMA system (Fig. S4A). The magnetic torque acting on the MARCE was tested using a torque transducer in our EMA system (Fig. S4B).

Locomotion resistance of MARCE

The locomotion resistance of MARCE in the intestines was measured using a tensile dynamometer connected via a thin wire and pulled by a linear stage (Fig. S7). To reflect different intestinal conditions, measurements were performed with MARCE placed on intestinal tissues and within collapsed intestines. A thin wire connected the tensile dynamometer to the MARCE, and a linear stage pulled the dynamometer at speeds of 5, 10, and 20 mm/s. Each test was repeated 5 times, and the maximum value from each group was recorded.

Locomotion test of MARCE

The locomotion of the MARCE was driven by a self-developed EMA system (Figs. 3a and S11). The EMA system was controlled via a joystick connected to a computer, which processed the input signal using LabVIEW software and sent output signals through an I/O device to digital servo amplifiers. Powered by DC sources, these amplifiers drove electromagnetic coils to generate a magnetic field. A camera monitored the magnetically driven MARCE for real-time adjustments.

Drug release test

Epinephrine-loaded microneedle patches were applied to seven segments of intestinal tissue, and removed after 5, 10, 15, 30, 60, 120, and 300 s, respectively. The tissues were homogenized using a tissue grinder (SCIENTZ-24, SCIENTZ, China), phosphate buffer (pH 7.3) was then added and sonicated for 2 min. Sample absorbance was measured at 279 nm using a UV-Vis-NIR spectrophotometer (UV-3600i plus, SHIMADZU, Japan). Epinephrine content was determined by comparing the absorbance values to a standard calibration curve. After 300 s, the microneedle patches had fully dissolved, indicating the total drug load. All experiments were performed in triplicate.

Ex vivo test

Intestine phantom test

A transparent, curved intestinal phantom model was constructed by 3D printing. Its inner surface was covered with wet porcine intestinal tissue to mimic the small intestine. Two red-dotted double-sided tapes were attached to mark target lesion locations. The phantom was placed within the EMA system, where the locomotion of MARCE was tracked by a camera and controlled in real time using magnetic fields generated by the EMA system.

Ex vivo intestine test

The ex vivo test was performed using a segment of swine small intestine. Red ink was injected to mark the target lesion locations. The intestine was placed within the effective working area of the EMA system, and the MARCE was placed in the small intestine. Driven by the magnetic field, MARCE successively delivered the microneedle patches to two target lesions. The kinematic illustration of the drug delivery process is presented in Fig. S12.

Finite element analysis

The magnetic field distributions of the EMA system for the magnetic actuation of the MARCE were analyzed using COMSOL Multiphysics (Version 6.2; COMSOL, Sweden), as shown in Fig. S3. The analysis and calculation employed the Magnetic Field physical module. The remanent flux density model was employed for the magnet, while the relative permeability model was used for air and coils. The recoil permeability and remanent flux density of the magnets were set to 1.05 and 1.44T, respectively. The relative permeability and permittivity of air and coils were assigned a value of 1. The 3D tetrahedral mesh model included: a magnetic spring (Fig. S3A) with a 60 mm air domain and magnet domains (air grid <1 mm, magnet A grid <0.2 mm, magnet B grid <0.03 mm); and Maxwell/Helmholtz coil models (Fig. S3B, C) with a 400 mm air domain, coils, and magnet (external air grid < 14 mm, internal air grid < 4 mm, coils grid < 3 mm, magnet grid < 2 mm respectively).

Acknowledgements

This research is financially supported by the National Natural Science Foundation of China (Project No. 52175386), the Natural Science Foundation of Guangdong Province (Project Nos. 2023A1515012634 and 2022B1515020011), the Shenzhen Science and Technology Program (Project Nos. JCYJ20220818102201003, KCXFZ20230731094500001, and JCYJ20220818102201002), the Science and Technology Program of Guangzhou, China (Project No. 2024B03J0121), and the Fundamental Research Funds for the Central Universities, Sun Yat-sen University (Project No. 24xkjc011).

Author details

[1]State Key Laboratory for High Performance Tools, Guangdong Provincial Key Laboratory of Minimally Invasive Surgical Instruments and Manufacturing Technology, School of Electromechanical Engineering, Guangdong University of Technology, Guangzhou, China. [2]School of Aeronautics and Astronautics, Shenzhen Campus of Sun Yat-sen University, Shenzhen, China. [3]Guangdong Provincial Key Laboratory of Sensor Technology and Biomedical Instrument, School of Biomedical Engineering, Shenzhen Campus of Sun Yat-sen University, Shenzhen, China. [4]State Key Laboratory of Optoelectronic Materials and Technologies, Guangdong Province Key Laboratory of Display Material and Technology, School of Electronics and Information Technology, Sun Yat-Sen University, Guangzhou, China

Author contributions

W.C. and J.S. conceived the idea; W.C., J.S., X.X., J.Z., L.J., and C.W. designed the research. W.C. and J.S. fabricated the MARCE and carried out force measurement experiments; W.C. and X.C. conducted locomotion and ex vivo studies. W.C. fabricated the microneedle patches with help from J.H. and Z.Y. W.C., F.C., K.Z., Y.L., X.L., and L.J. analyzed the experimental data and prepared figures. W.C., L.J., J.S., and J.Z. wrote the manuscript. L.J. and J.S. coordinated and supervised the research. All authors discuss the results and comment on the manuscript.

Data availability

The data presented in this work are available from the lead contact upon reasonable request. This study did not analyze code.

Competing interests

The authors declare no competing interests.

Supplementary information The online version contains supplementary material available at https://doi.org/10.1038/s41378-025-01145-5.

Received: 21 August 2025 Revised: 27 September 2025 Accepted: 24 October 2025
Published online: 26 January 2026

References

1. Peery, A. F. et al. Burden of gastrointestinal disease in the United States: 2012 update. *Gastroenterology* **143**, 1179–1187.e1173 (2012).
2. Simi, M., Gerboni, G., Menciassi, A. & Valdastri, P. Magnetic torsion spring mechanism for a wireless biopsy capsule. *J. Med. Dev.* **7**, 1–9 (2013).
3. Lamb, C. A. et al. British Society of Gastroenterology consensus guidelines on the management of inflammatory bowel disease in adults. *Gut* **68**, s1–s106 (2019).
4. Swain, C. P., Gong, F. & Mills, T. N. An endorobot for gastrointestinal endoscopy. *Gastrointest. Endosc.* **41**, 73 (1995).
5. Wang, A. et al. Wireless capsule endoscopy. *Gastrointest. Endosc.* **78**, 805–815 (2013).
6. Iddan, G., Meron, G., Glukhovsky, A. & Swain, P. Wireless capsule endoscopy. *Nature* **405**, 417–417 (2000).
7. Enns, R. A. et al. Clinical practice guidelines for the use of video capsule endoscopy. *Gastroenterology* **152**, 497–514 (2017).
8. Vasilakakis, M. et al. Follow-up on: optimizing lesion detection in small bowel capsule endoscopy and beyond: from present problems to future solutions. *Expert Rev. Gastroenterol. Hepatol.* **13**, 129–141 (2019).
9. Chen, W. Y., Sui, J. B. & Wang, C. Y. Magnetically actuated capsule robots: a review. *IEEE Access* **10**, 88398–88420 (2022).
10. Tortora, G. et al. An ingestible capsule for the photodynamic therapy of Helicobacter pylori infection. *IEEE ASME Trans. Mechatron.* **21**, 1935–1942 (2016).
11. Valdastri, P. et al. Wireless therapeutic endoscopic capsule: in vivo experiment. *Endoscopy* **40**, 979–982 (2008).
12. Leung, B. H. K. et al. A therapeutic wireless capsule for treatment of gastrointestinal haemorrhage by balloon tamponade effect. *IEEE Trans. Biomed. Eng.* **64**, 1106–1114 (2017).
13. Dhalla, A. K. et al. A robotic pill for oral delivery of biotherapeutics: safety, tolerability, and performance in healthy subjects. *Drug Deliv. Transl. Res.* **12**, 294–305 (2021).
14. Abramson, A. et al. An ingestible self-orienting system for oral delivery of macromolecules. *Science* **363**, 611–615 (2019).
15. Abramson, A. et al. Oral delivery of systemic monoclonal antibodies, peptides and small molecules using gastric auto-injectors. *Nat. Biotechnol.* **40**, 103–109 (2021).
16. Arrick, G. et al. Cephalopod-inspired jetting devices for gastrointestinal drug delivery. *Nature* **636**, 481–487 (2024).
17. Le, V. H. et al. A soft-magnet-based drug-delivery module for active locomotive intestinal capsule endoscopy using an electromagnetic actuation system. *Sens Actuators A Phys.* **243**, 81–89 (2016).
18. Sun, Y. et al. Magnetically driven capsules with multimodal response and multifunctionality for biomedical applications. *Nat. Commun.* **15**, 1839 (2024).
19. Yim, S., Goyal, K. & Sitti, M. Magnetically actuated soft capsule with the multimodal drug release function. *IEEE ASME Trans. Mechatron.* **18**, 1413–1418 (2013).
20. Hua, D. et al. Design, fabrication, and testing of a novel ferrofluid soft capsule robot. *IEEE-ASME Trans. Mechatron.* **27**, 1403–1413 (2022).
21. Song, S. et al. Integrated design and decoupled control of anchoring and drug release for wireless capsule robots. *IEEE ASME Trans. Mechatron.* **27**, 2897–2907 (2021).
22. Wang, Z. et al. Selective motion control of a novel magnetic-driven minirobot with targeted drug sustained-release function. *IEEE ASME Trans. Mechatron.* **27**, 336–347 (2022).
23. Munoz, F., Alici, G., Zhou, H., Li, W. & Sitti, M. Analysis of magnetic interaction in remotely controlled magnetic devices and its application to a capsule robot for drug delivery. *IEEE ASME Trans. Mechatron.* **23**, 298–310 (2018).
24. Jensen, D. M., Machicado, G. A., Jutabha, R. & Kovacs, T. O. Urgent colonoscopy for the diagnosis and treatment of severe diverticular hemorrhage. *N. Engl. J. Med.* **342**, 78–82 (2000).
25. Chetcuti Zammit, S. et al. Overview of small bowel angioectasias: clinical presentation and treatment options. *Expert Rev. Gastroenterol. Hepatol.* **12**, 125–139 (2018).
26. Byrne, J. et al. Devices for drug delivery in the gastrointestinal tract: a review of systems physically interacting with the mucosa for enhanced delivery. *Adv. Drug Deliv. Rev.* **177**, 113926 (2021).
27. Zhang, X., Chen, G., Fu, X., Wang, Y. & Zhao, Y. Magneto-responsive microneedle robots for intestinal macromolecule delivery. *Adv. Mater.* **33**, e2104932 (2021).
28. Abramson, A. et al. A luminal unfolding microneedle injector for oral delivery of macromolecules. *Nat. Med.* **25**, 1512–1518 (2019).
29. Chen, W. et al. Dynamic omnidirectional adhesive microneedle system for oral macromolecular drug delivery. *Sci. Adv.* **8**, eabk1792 (2022).
30. Levy, J. A., Straker, M. A., Stine, J. M., Beardslee, L. A., & Ghodssi, R. Magnetically triggered ingestible capsule for localized microneedle drug delivery. *Device* **2**, 100438 (2024).
31. Lee, J., Lee, H., Kwon, S. H. & Park, S. Active delivery of multi-layer drug-loaded microneedle patches using magnetically driven capsule. *Med. Eng. Phys.* **85**, 87–96 (2020).
32. Lee, J., Sohn, S. W., Lee, H. & Park, S. Open-close mechanism of magnetically actuated capsule for multiple hemostatic microneedle patch delivery. *Int. J. Control Autom. Syst.* **20**, 2285–2296 (2022).
33. Gittard, S. D. et al. Fabrication of polymer microneedles using a two-photon polymerization and micromolding process. *J. Diab. Sci. Technol.* **3**, 304–311 (2009).
34. Gittard, S. D. et al. The effects of geometry on skin penetration and failure of polymer microneedles. *J. Adhes. Sci. Technol.* **27**, 227–243 (2013).
35. Boley, S. J. et al. On the nature and etiology of vascular ectasias of the colon. *Gastroenterology* **72**, 650–660 (1977).
36. Diggs, N. G., Holub, J. L., Lieberman, D. A., Eisen, G. M. & Strate, L. L. Factors that contribute to blood loss in patients with colonic angiodysplasia from a population-based study. *Clin. Gastroenterol. Hepatol.* **9**, 415–420 (2011).
37. Nojkov, B. & Cappell, M. S. Gastrointestinal bleeding from Dieulafoy's lesion: clinical presentation, endoscopic findings, and endoscopic therapy. *World J. Gastrointest. Endosc.* **7**, 295–307 (2015).
38. Wallace, M. B., Fockens, P., & Sung, J. J.-Y. *Gastroenterological Endoscopy*, Thieme, ed. 3rd (2018).
39. Kruss, S. et al. Stimulation of cell adhesion at nanostructured Teflon interfaces. *Adv. Mater.* **22**, 5499–5506 (2010).
40. Lambert, G. P. et al. Selected contribution: hyperthermia-induced intestinal permeability and the role of oxidative and nitrosative stress. *J. Appl Physiol.* **92**, 1750–1761 (2002).